Catalysis Today 175 (2011) 534–540

Contents lists available at ScienceDirect

Catalysis Today

journal homepage: www.elsevier.com/locate/cattod

Transformation of crystalline heteronuclear cyano complex to crystalline perovskite-type oxide by thermal decomposition

Makiko Asamoto, Masataka Hino, Syuhei Yamaguchi, Hidenori Yahiro*

Department of Materials Science and Biotechnology, Graduate School of Science and Engineering, Ehime University, Matsuyama 790-8577, Japan

ARTICLE INFO

Article history:
Received 31 October 2010
Received in revised form 17 April 2011
Accepted 25 April 2011
Available online 2 June 2011

Keywords:
Perovskite-type oxide
Heteronuclear cyano complex
Thermal decomposition
CO oxidation

ABSTRACT

The thermal decomposition reaction of crystalline heteronuclear cyano complex precursor to crystalline perovskite-type oxide catalyst was investigated. From X-ray single crystal analysis and XRD, FT-IR, TG-DTA, SEM, and BET measurements, the thermal decomposition process of $Sm[Fe(CN)_6]\cdot 4H_2O$ precursor was elucidated. It was found that the specific surface area of $SmFeO_3$ decreased monotonously with increasing calcination temperature of $Sm[Fe(CN)_6]\cdot 4H_2O$, while the highest catalytic activity for CO oxidation was achieved for $Sm[Fe(CN)_6]\cdot 4H_2O$ calcined at 600 °C. The size of $Sm[Fe(CN)_6]\cdot 4H_2O$ precursor depended on the molar concentration of starting materials, $Sm(NO_3)_3\cdot 6H_2O$ and $K_3Fe(CN)_6$, in aqueous solution (C_s); the size of $Sm[Fe(CN)_6]\cdot 4H_2O$ decreased with decreasing C_s. The decrease in particle size of cyano complex was found to result in the increase in specific surface area of perovksite-type oxide obtained after calcination.

1. Introduction

Perovskite-type oxide with general formula, ABO_3, in which A is usually an alkaline earth metal ion or a lanthanoid ion and B is a transition metal ion, is one of the compounds used in the environmental friendly catalytic systems. Several perovskite-type oxides have been reported to show high catalytic activity for oxidations of hydrocarbon [1,2] and chlorinated volatile organic compounds [3] and decomposition of NO [4–6]. Traditionally, perovskite-type oxides have been prepared by solid-state reaction of oxides and/or carbonates [7–9]. However, this traditional method offers the disadvantages of long processing time, low surface area, large particle size, and limited degree of chemical homogeneity. In general, wet-chemical methods are available to prepare finer and more homogeneous powders at relatively low temperature. Up to date, numerous efforts of low temperature wet-chemical method have been undertaken to increase the surface area of perovskite-type oxide. For example, sol–gel [8,10–12], co-precipitaion [7,10,13], citrate route [7,8], reverse micelle [14,15], reverse homogeneous precipitation [16], and polymeric precursor methods [17,18], and flame hydrolysis of aqueous solution of precursor salts [19] have been developed and designed to prepare nano-sized perovskite-type oxides. However, the development of simple and low-cost procedures for obtaining single-phase perovskite-type oxide nanoparticles with a homogeneous chemical composition under mild condition is still needed.

Sadaoka and co-workers [20–27] reported the new preparation route of perovskite-type oxide via the thermal decomposition of heteronuclear cyano complex, $Ln[M(CN)_6]\cdot nH_2O$ (abbreviated as CN method). Recently, we have prepared $SmFe_{0.5}Co_{0.5}O_3$ catalyst by CN method and found that this catalyst exhibited the highest CO conversion among a series of $SmFe_xCo_{1-x}O_3$ catalysts. This result demonstrated that there is a remarkable synergistic effect by co-existing B site cations on the catalytic activities of CO oxidation for $SmFe_xCo_{1-x}O_3$ catalysts due to high homogeneity in composition [28]. Thus, CN method possesses advantages for preparing perovskite-type oxide active for catalytic CO oxidation; however, little is known about the formation mechanism of crystalline perovskite-type oxide from crystalline cyano complex by thermal decomposition. In the present study, the thermal decomposition process of simple cyano complex, $Sm[Fe(CN)_6]\cdot nH_2O$, was investigated by characterizing both the synthesized cyano complexes and the obtained perovskite-type oxides using X-ray single crystal structure analysis, powder X-ray diffraction (XRD), Fourier-transformed infrared spectroscopy (FT-IR), BET measurement, scanning electron microscopy (SEM), and thermal analysis (TG-DTA). In addition, the catalytic activity of CO oxidation was evaluated for perovskite-type oxide prepared by CN method.

2. Experimental

The cyano metal complex, $Sm[Fe(CN)_6]\cdot nH_2O$, was synthesized as a precursor of perovskite-type oxide [21]. All chemicals were

* Corresponding author. Tel.: +81 89 927 9929; fax: +81 89 927 9946.
E-mail address: hyahiro@eng.ehime-u.ac.jp (H. Yahiro).

0920-5861/$ – see front matter © 2011 Elsevier B.V. All rights reserved.
doi:10.1016/j.cattod.2011.04.048

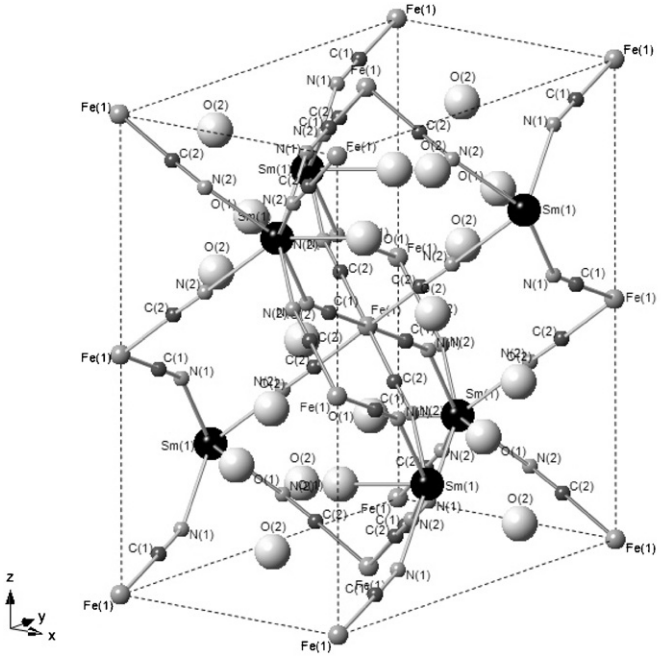

Fig. 1. Crystal structure of $Sm[Fe(CN)_6]\cdot 4H_2O$ complex.

Table 1
Crystallographic data for $Sm[Fe(CN)_6]\cdot 4H_2O$.

Empirical formula	$C_6H_8FeN_6O_4Sm$
Formula weight	434.41
Crystal system	Orthorhombic
Space group	*Cmcm* (No. 63)
a (Å)	7.444(2)
b (Å)	12.817(4)
c (Å)	13.688(4)
V (Å^3)	1306.0(6)
z	4
D_{calcd} (g cm^{-3})	2.168
F_{000}	792.00
μ(Mo Kα) (cm^{-1})	55.855
λ (Å)	0.7107
T (°C)	−173
No. of refls. measured	1113
No. of refls. used ($I > 2.0\sigma(I)$)	52
R_1 [a]/R_w [b]	0.0265/0.0757
Goodness of fit indicator	1.197

[a] $R_1 = \Sigma\,||F_o| - |F_c||/\Sigma\,|F_o|$.

[b] $R_w = [\,\Sigma(w(F_o^2 - F_c^2)^2)/\Sigma w(F_o^2)^2\,]^{1/2}$.

Table 2
Selected bond lengths (Å) and angles (°) for $Sm[Fe(CN)_6]\cdot 4H_2O$.

Bond length (Å)			
Sm(1)–O(1)	2.397(2)	Sm(1)–N(1)	2.530(4)
Sm(1)–N(2)	2.499(2)	Fe(1)–C(1)	1.932(3)
Fe(1)–C(2)	1.930(2)	N(1)–C(1)	1.150(5)
N(2)–C(2)	1.154(3)	O(1)–O(2)	2.803(3)
Bond angle (°)			
O(1)–Sm(1)–O(1)	108.31(9)	O(1)–Sm(1)–N(1)	71.97(5)
O(1)–Sm(1)–N(2)	79.54(7)	O(1)–Sm(1)–N(2)	142.78(6)
N(1)–Sm(1)–N(1)	116.20(12)	N(1)–Sm(1)–N(2)	141.93(6)
N(1)–Sm(1)–N(2)	76.56(9)	N(2)–Sm(1)–N(2)	73.82(8)
N(2)–Sm(1)–N(2)	74.19(8)	C(1)–Fe(1)–C(1)	180.00(17)
C(1)–Fe(1)–C(2)	91.23(11)	C(1)–Fe(1)–C(2)	88.77(11)
C(1)–Fe(1)–C(2)	88.76(11)	C(2)–Fe(1)–C(2)	89.15(11)
C(2)–Fe(1)–C(2)	90.85(11)	Sm(1)–N(1)–C(1)	147.2(3)
Sm(1)–N(2)–C(2)	166.1(2)	Fe(1)–C(1)–N(1)	178.6(3)
Fe(1)–C(2)–N(2)	178.1(2)		

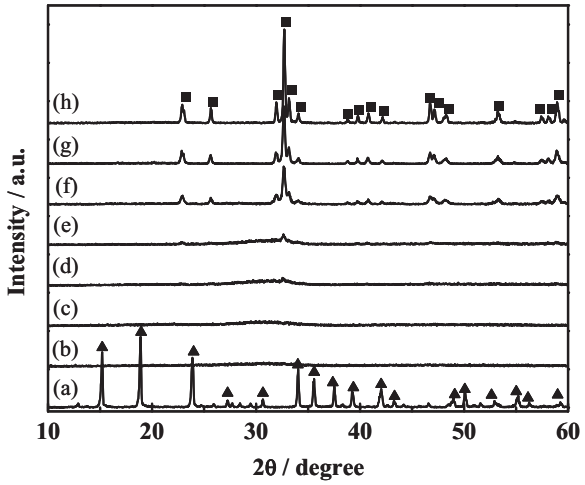

Fig. 2. XRD patterns of $Sm[Fe(CN)_6]\cdot 4H_2O$ complex (a) as-prepared, (b) preheated at 300 °C for 2 h, and then calcined at (c) 400 °C for 5 h, (d) 600 °C for 1 h, (e) 600 °C for 2 h, (f) 600 °C for 5 h, (g) 800 °C for 5 h, and (h) 1000 °C for 5 h after heat treatment (b). (▲) $Sm[Fe(CN)_6]\cdot 4H_2O$ and (■) $SmFeO_3$.

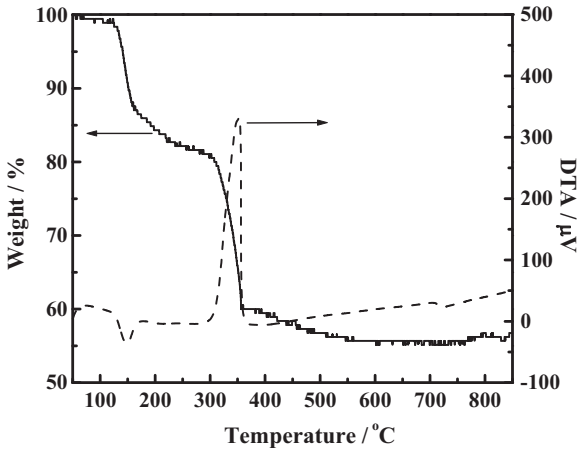

Fig. 3. TG-DTA curves of $Sm[Fe(CN)_6]\cdot 4H_2O$ complex. The solid and dotted lines stand for TG and DTA curves, respectively.

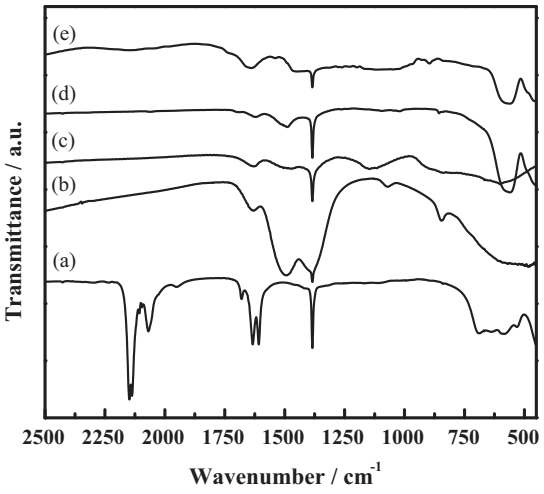

Fig. 4. FT-IR spectra of heteronuclear cyano complexes, $Sm[Fe(CN)_6]\cdot 4H_2O$, (a) as-prepared, (b) pretreated at 300 °C for 2 h, and calcined at (c) 400 °C, (d) 600 °C, and (e) 800 °C for 5 h. The band at 1385 cm^{-1} originates from KBr powder.

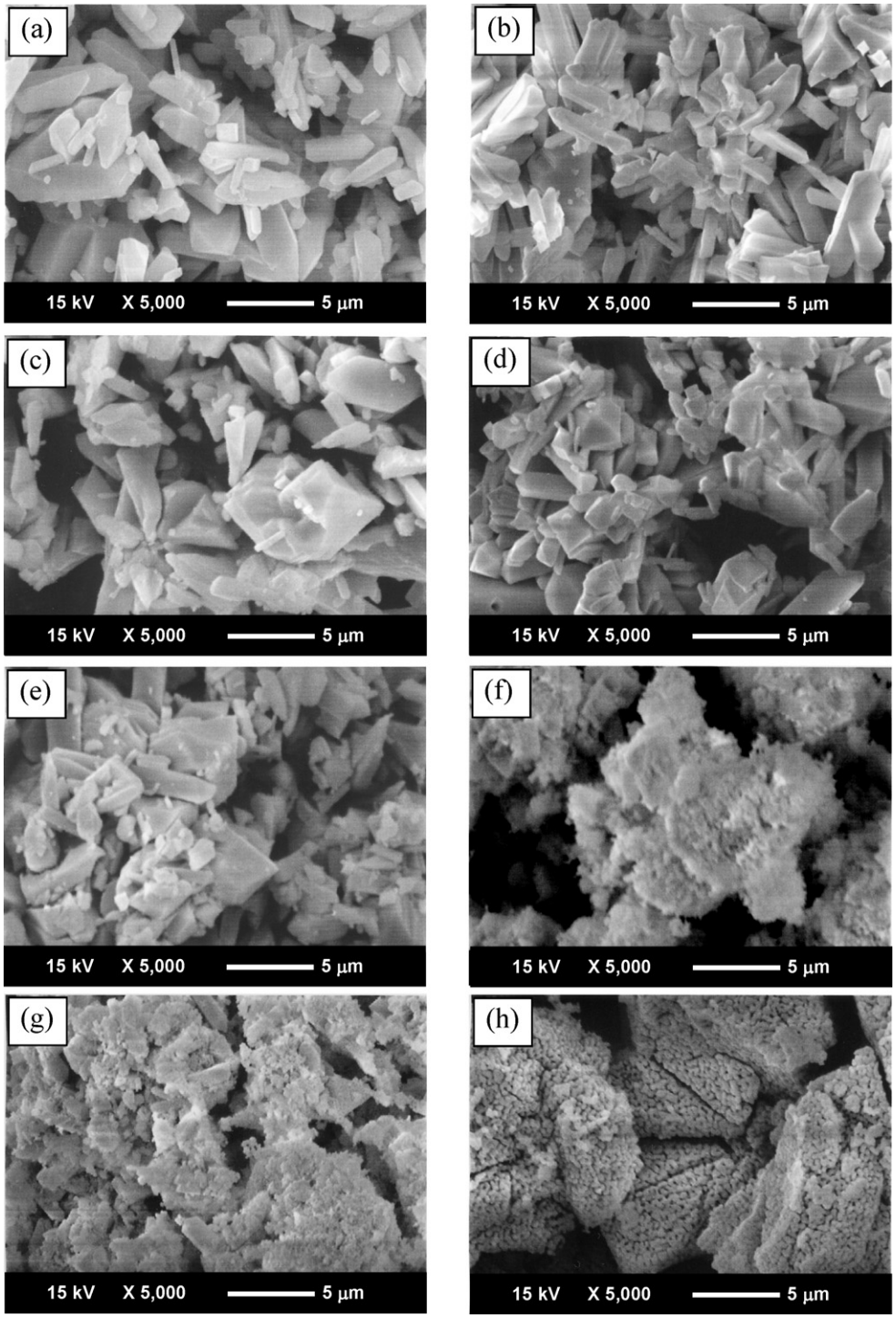

Fig. 5. SEM images of the heteronuclear cyano complexes, $Sm[Fe(CN)_6]\cdot 4H_2O$, (a) as-prepared, (b) preheated at 300 °C for 2 h, calcined at (c) 400 °C for 5 h, (d) 600 °C for 1 h, (e) 600 °C for 2 h, (f) 600 °C for 5 h, (g) 800 °C for 5 h, and (h) 1000 °C for 5 h.

used without any purification. Aqueous solutions of appropriate amounts of $Sm(NO_3)_3\cdot 6H_2O$ (Wako, 99.5%) and $K_3Fe(CN)_6$ (Hayashi, 99.0%) were mixed at room temperature by continuous stirring for 0.5 h, resulting in the formation of $Sm[Fe(CN)_6]\cdot nH_2O$ according to the following reaction:

$$Sm(NO_3)_3(aq) + K_3Fe(CN)_6(aq) \rightarrow Sm[Fe(CN)_6]\cdot nH_2O(s) + 3KNO_3(aq)$$

The resulting precipitate was collected by suction filtration, washed with deionized water, ethanol, and diethyl ether, and then air-dried at 50 °C. The obtained powder was preheated at 300 °C for 2 h and then calcined in air at 400–1000 °C for 1–5 h to yield perovskite-type oxide, $SmFeO_3$.

X-ray single crystal diffraction measurement was made on a Rigaku VariMax Saturn CCD 724+ diffractometer with graphite monochromated Mo Kα radiation at −173 °C. Data were collected and processed using Crystal Clear [29] for windows software. Neutral scattering factors were obtained from standard source. In the reduction of data, Lorentz and polarization corrections were carried out. The structural analysis was performed using Crystal Structure [30] for windows software. All structures were solved by SIR2004

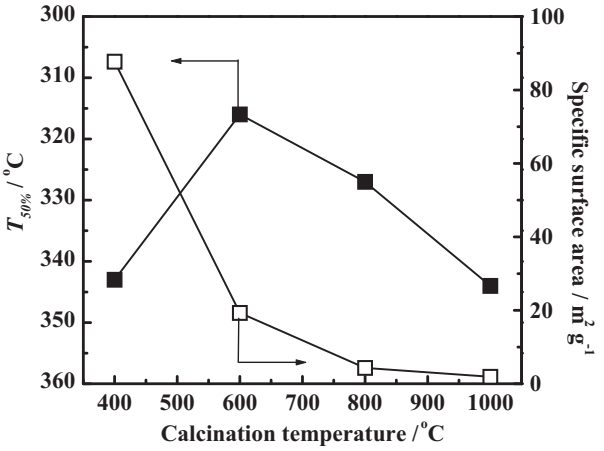

Fig. 6. Catalytic activities ($T_{50\%}$; ■) and specific surface area (□) as a function of calcination temperature. The perovskite-type oxide catalyst (0.5 g) was pre-treated in flowing helium gas at 500 °C. The reaction gas contained 1.0 vol% of CO, 20.0 vol% of O_2, and helium as a balance gas. The total flow rate was 50 cm^3 min^{-1}. $T_{50\%}$ is defined as the temperature giving 50% CO-conversion.

[31] (direct methods) and refined by SHELX-97 [32]. The powder XRD patterns of products were collected on a Rigaku MiniFlex II diffractometer using Cu Kα radiation. The thermal decomposition process of complex was studied by thermogravimetry and differential thermal analysis (TG-DTA; DTG-60E, Shimazu), performed at a heating rate of 10 °C min^{-1} in air. FT-IR spectra of samples with KBr powder were recorded with a PerkinElmer Spectrum One spectrometer. To measure the distributions and the mean particle sizes (d_{av}), the cyano complexes and the perovskite-type oxides were observed by SEM (JSM-5310, JEOL). The specific surface area was determined with the BET analysis (Belsorp-mini, BEL Japan) for the adsorption–desorption property measurements using N_2 adsorbent at −196 °C.

The catalytic reaction of CO oxidation was carried out in a conventional fixed-bed flow reactor [28]. The perovskite-type oxide catalyst (0.5 g) was placed in the flow reactor and pre-treated in flowing helium gas at 500 °C. The reaction gas contained 1.0 vol% of CO, 20.0 vol% of O_2, and helium as a balance gas. The total flow rate was 50 cm^3 min^{-1}. The reaction temperature was increased stepwise from 50 to 450 °C, and the reaction was carried out at each temperature until the conversion reached a constant value. The gas composition was analyzed by gas chromatography (GC-8AIT, Shimazu) using Molecular Sieve 5A column. The catalytic activity for CO oxidation was evaluated by conversion of CO ($=([CO]_{out}/[CO]_{in}) \times 100$).

3. Results and discussion

3.1. Thermal decomposition process of $Sm[Fe(CN)_6]\cdot nH_2O$

The crystallographic data of prepared heterocyano-complex, $Sm[Fe(CN)_6]\cdot nH_2O$, as a precursor of perovskite-type oxide, were obtained by a single crystal X-ray analysis. Fig. 1 shows the crystal structure of $Sm[Fe(CN)_6]\cdot nH_2O$ with orthorhombic space group *Cmcm* (a = 7.444(2) Å, b = 12.817(4) Å, c = 13.688(4) Å, V = 1306.0(6) $Å^3$, and Z = 4). The crystallographic data are summarized in Table 1 and selected bond lengths and angles are given in Table 2. A samarium ion is eight coordinate; two oxygen atoms in crystal waters and six nitrogen atoms in CN groups are coordinated to a samarium atom in square antiprismatic geometry. On the other hand, six carbon atoms are coordinated to an iron atom in octahedral geometry. As can be seen in Table 1 and Fig. 1, the number of crystal water in unit cell, n, is determined to be 4, being in good agreement with TG-DTA result (vide infra). In addition, the uncoordinated crystal water molecules may be hydrogen-bonded to a crystal water coordinated to a samarium atom because the bond length of O(1)–O(2) is 2.803(3) Å. A similar crystallographic result was reported by Zhou et al. [33].

Fig. 2 shows XRD profiles of $Sm[Fe(CN)_6]\cdot 4H_2O$ complexes preheated at 300 °C for 2 h in air, followed by calcined at 400–1000 °C for 1–5 h in air. It is demonstrated from XRD analysis that as-prepared $Sm[Fe(CN)_6]\cdot 4H_2O$ complex possesses orthorhombic structure [34]. When $Sm[Fe(CN)_6]\cdot 4H_2O$ complex was preheated at 300 °C for 2 h in air, XRD peaks due to the orthorhombic structure of $Sm[Fe(CN)_6]\cdot 4H_2O$ disappeared completely. No strong peak was observed in the calcination temperature range of 300–400 °C except for the hallow peak centered at *ca.* 31°. Therefore, the sample calcined at 300–400 °C was found to be in an amorphous phase and/or an assembly consisting of nanoparticles (<1 nm) with size below detectable level by XRD analysis. When the sample was calcined at 600 °C, the peaks assigned to orthorhombic structure of perovskite-type oxide, $SmFeO_3$, newly appeared [34] and their intensities increased with increasing calcination time (Fig. 2(d)–(f)) and calcination temperature (Fig. 2(g) and (h)). This indicates that the crystal growth of perovskite-type oxide successively proceeds in the temperature range between 600 and 1000 °C.

TG-DTA and IR measurements were performed for further understanding the influence of calcination temperature. Fig. 3 shows TG-DTA curves of $Sm[Fe(CN)_6]\cdot 4H_2O$ complex measured in flowing air. The two large weight losses in TG curve were observed at 100–200 and 300–400 °C, being accompanied by endothermic and exothermic effects, respectively, in DTA curve. These two weight losses may be due to desorption of H_2O for 100–200 °C and oxidation of CN groups for 300–400 °C. A similar result was observed for $Sm[Co(CN)_6]\cdot nH_2O$ complex [35]. The small weight loss was additionally observed at 400–600 °C. This may come from desorption of CO_2 and/or NO_x produced by the decomposition of surface carbonate and nitrate species derived from oxidation of CN groups.

Fig. 4 shows FT-IR spectra of $Sm[Fe(CN)_6]\cdot 4H_2O$ as-prepared, preheated at 300 °C for 2 h, and calcined at 400–800 °C for 5 h. For the as-prepared $Sm[Fe(CN)_6]\cdot 4H_2O$ complex, CN stretching bands were clearly observed at about 2145 and 2067 cm^{-1} [36]. In addition, the bands related to the bending vibration of the different crystal waters in complex were observed in the range of 1600–1630 cm^{-1} [37]. When $Sm[Fe(CN)_6]\cdot 4H_2O$ complex was preheated at 300 °C for 2 h in air, the bands due to CN stretching and H_2O bending vibrations disappeared, as can be seen in Fig. 4(b). This result is in agreement with TG-DTA result that crystal water in complex was desorbed below 200 °C and CN groups were oxidized at 300–400 °C. It should be noted that the bands attributed to carbonate and/or nitrate groups were newly observed at 1300–1500, 1075, and 840 cm^{-1} [26]. Our previous in situ DRIFT-IR study of calcined $Sm[Fe(CN)_6]\cdot 4H_2O$ demonstrated that at least two types of carbonate species were formed by thermal decomposition of cyano complex; one is the bidentate-type carbonate produced by oxidation of CN groups and the other is the monodentate-type carbonate formed by CO_2 adsorption [35], although such carbonates could not distinguish from the present IR spectra. Nitrate species undoubtedly come from oxidation of CN groups in $Sm[Fe(CN)_6]\cdot 4H_2O$.

The band intensities of carbonate and nitrate species decreased with increasing calcination temperature (Fig. 4(c)–(e)). When $Sm[Fe(CN)_6]\cdot 4H_2O$ complex was calcined at 600 °C (Fig. 4(d)), the intense bands appeared at 560 and 450 cm^{-1}. These bands can be assigned to the Fe–O stretching and bending vibrations of octahedral FeO_6, supporting the formation of perovskite-type structure [36].

From the present XRD, TG-DTA, and IR results, the thermal decomposition process of $Sm[Fe(CN)_6]\cdot 4H_2O$ may be proposed

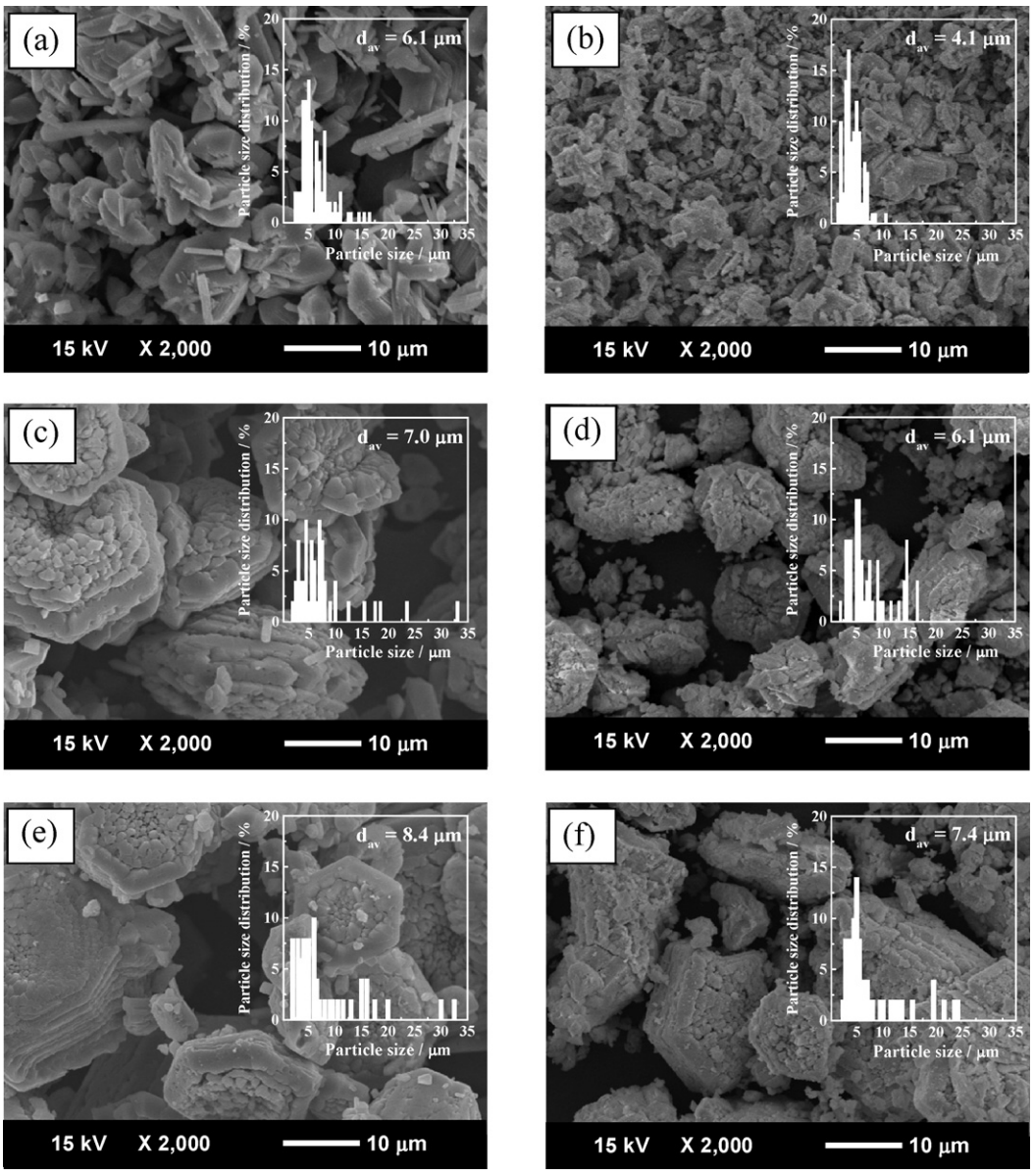

Fig. 7. SEM images and particle size distributions of the heteronuclear cyano complexes, $Sm[Fe(CN)_6]\cdot 4H_2O$, synthesized from the aqueous solution with concentration of (a) 0.2 M, (c) 0.6 M, and (e) 1.0 M. SEM images (b), (d), and (f) are of the perovskite-type oxides, $SmFeO_3$, prepared by calcination of (a), (c), and (e) complexes, respectively, at 700 °C for 1 h.

as follows. (1) When $Sm[Fe(CN)_6]\cdot 4H_2O$ is calcined at <300 °C, the desorption of crystal water initially occurs and CN groups in cyano complex are oxidized to form amorphous particle and/or nanoparticle assembly of perovskite-type oxide, probably covered by carbonate and nitrate species. (2) At >600 °C of calcination temperature, CO_2 and NO_x produced by decomposition of carbonate and nitrate species are desorbed and simultaneously the crystal growth of perovskite-type oxide starts to proceed.

Fig. 5 shows SEM images of $Sm[Fe(CN)_6]\cdot 4H_2O$ preheated at 300 °C and calcined at 400–1000 °C. For as-prepared $Sm[Fe(CN)_6]\cdot 4H_2O$ complex, the particle size (2–20 μm) was much larger than the crystallite size estimated from XRD diffraction line using Scherer's equation (46 nm). This suggests that as-prepared cyano complex shown in Fig. 5(a) is polycrystalline particle. The particle sizes as well as shapes were essentially the same as those of $Sm[Fe(CN)_6]\cdot 4H_2O$ complex calcined at 300–400 °C (Fig. 5(b) and (c)) although CN groups were oxidized as demonstrated by TG-DTA measurement (vide supra). When the sample was calcined at 600 °C, the progressive change in the morphology of particle was observed with calcination time. Clearly, the sample calcined at 600 °C showed the powder deposition on the surface of each particle, probably due to the surface diffusion for crystal growth like normally observed for powder-sintering. Such a crystal growth was supported by XRD result that the diffraction peaks assigned to perovskite-type oxide were observed at 600 °C, as shown in Fig. 2. With further increasing calcination temperature, the assembly consisting of small particles was observed as shown in Fig. 5(h).

The catalytic activities of CO oxidation were measured for $Sm[Fe(CN)_6]\cdot 4H_2O$ calcined at 400–1000 °C for 5 h. Fig. 6 shows catalytic activities and specific surface areas as a function of calcination temperature. The specific surface area decreased monotonously with increasing calcination temperature. The specific surface area of $SmFeO_3$ calcined at 600 °C (*ca.* 20 $m^2\,g^{-1}$) was comparable to that calcined at the same temperature in the other preparation methods (11–17 $m^2\,g^{-1}$) [38]. In contrast to the specific surface area, the catalytic activity of CO oxidation exhibited the maximal value at 600 °C of calcination temperature. This suggests that the catalytic activity depended on not only specific surface area but also another

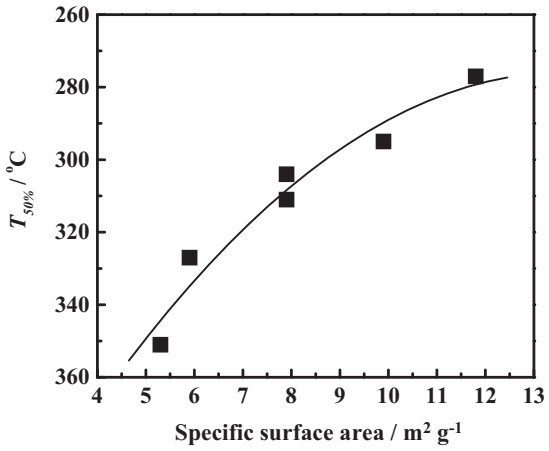

Fig. 8. Catalytic activities ($T_{50\%}$; ■) of $SmFeO_3$ prepared by CN method as a function of specific surface area. Calcination temperature was 700 °C.

factor. The specific surface area of the sample calcined at 400 °C was very high, whereas it showed no XRD peak due to perovskite-type oxide, as shown in Fig. 2(c). Therefore, the formation of crystalline perovskite-type may be also important for obtaining high catalytic activity.

3.2. Preparation of $Sm[Fe(CN)_6]\cdot 4H_2O$ precursor

As mentioned in previous section, it is important to prepare the perovskite-type oxide with both high specific surface area and high crystallinity to improve catalytic activity. In the case of general preparation methods such as sol–gel and co-precipitation methods, the specific surface area of perovskite-type oxide is controlled by calcination temperature of amorphous precursor; that is, lower calcination temperature, higher specific surface area [7,8,10]. In the present study, the control of the specific surface area of perovskite-type oxide was attempted by changing the preparation condition of crystalline cyano complex precursor. The resulting precursor was calcined at 700 °C for 1 h to yield the perovskite-type oxide with high crystallinity.

Fig. 7 shows SEM images of the $Sm[Fe(CN)_6]\cdot 4H_2O$ complex synthesized from aqueous solutions with different molar concentration of starting materials; $Sm(NO_3)_3\cdot 6H_2O$ and $K_3Fe(CN)_6$. The shape and size of cyano complex were dependent on the concentration of starting materials (C_s). The synthesis from aqueous solution with low C_s gave rod-like particle (Fig. 7(a)), while that with high C_s gave hexagonal column-like particle (Fig. 7(c) and (e)). Additionally, the flake particles with 2–5 μm were observed regardless of C_s and the number of their particles increased with increasing C_s. The insets of Fig. 7 represent the particle size distributions of each cyano complex. The mean particle sizes were 6.1, 7.0, and 8.4 μm for cyano complexes synthesized from the aqueous solution with C_s = 0.2, 0.6, and 1.0 M, respectively. The mean particle size of cyano complex increased with increasing C_s.

The SEM images and the particle size distributions of perovskite-type oxides prepared from each cyano complex are shown in Fig. 7(b), (d), and (e). The mean particle sizes of perovskite-type oxides increased with increasing C_s: 4.1, 6.1, and 7.4 μm for 0.2, 0.6, and 1.0 M, respectively. The size of $Sm[Fe(CN)_6]\cdot 4H_2O$ particles (Fig. 7(a), (c), and (e)) was slightly larger that of perovskite-type oxide (Fig. 7(b), (d), and (f)) because of the contraction of lattice volume in the transformation from a cyano complex to a perovskite-type oxide. From these results, it was concluded that the synthesis of cyano complex with small particle size is effective to obtain the perovsktie-type oxide with small particle size, giving the perovsktie-type oxide with large specific surface area. In fact, the BET specific surface area of $SmFeO_3$ prepared from cyano complex synthesized with C_s = 0.2 M (10 $m^2\ g^{-1}$) was larger than that with C_s = 1.0 M (5.3 $m^2\ g^{-1}$).

Fig. 8 shows the correlation between catalytic activity ($T_{50\%}$) and BET specific surface area of $SmFeO_3$ prepared from cyano complex synthesized with different C_s. The catalytic activity of $SmFeO_3$ monotonously increased with increasing specific surface area. Therefore, if cyano complex with small particle size can be synthesized, the perovskite-type oxide with large surface area can be obtained, resulting in high catalytic activity.

4. Conclusion

The thermal decomposition reaction of heteronuclear cyano complex, $Sm[Fe(CN)_6]\cdot 4H_2O$, to yield single-phase perovskite-type oxide, $SmFeO_3$ was investigated by X-ray single crystal analysis and XRD, FT-IR, TG-DTA, SEM, and BET specific surface area measurements. The single crystal X-ray analysis provided that $Sm[Fe(CN)_6]\cdot nH_2O$ possessed an orthorhombic structure (*Cmcm*) with lattice parameters: a = 7.444(2) Å, b = 12.817(4) Å, and c = 13.688(4) Å. From XRD, TG-DTA, and IR results, the thermal decomposition process of $Sm[Fe(CN)_6]\cdot 4H_2O$ complex was proposed as follows: when $Sm[Fe(CN)_6]\cdot 4H_2O$ was calcined at 300 °C, the desorption of crystal water initially occurred and CN groups in cyano complex were oxidized to form amorphous particles or the assembly of oxide nanoparticles covered by carbonate and nitrate species. At >600 °C of calcination temperature, CO_2 and NO_x were desorbed by decomposition of carbonate and nitrate species and simultaneously the crystalline growth of perovskite-type oxide took place. The surface area decreased monotonously with increasing calcination temperature, while the highest catalytic activity for CO oxidation was achieved for the sample calcined at 600 °C.

The shape and size of $Sm[Fe(CN)_6]\cdot 4H_2O$ precursor significantly depended on the concentration of starting materials in aqueous solution (C_s); the particle size of $Sm[Fe(CN)_6]\cdot 4H_2O$ decreased with decreasing C_s. The decrease in particle size of cyano complex was found to result in the increase in specific surface area of perovksite-type oxide obtained after calcination.

Supplementary data

Crystallographic information for $Sm[Fe(CN)_6]\cdot 4H_2O$ is available as CCDC798434 from the Cambridge Crystallographic Data Centre (CCDC). These data may be obtained from the CCDC via the web link www.ccdc.cam.ac.uk/data_request/cif.

Acknowledgements

This work was supported by a Grant-in-Aid for Scientific Research (B) (No. 21360397) and the Nissan Foundation.

References

[1] D.W. Johnson Jr., P.K. Gallagher, G.K. Wertheim, E.M. Vogel, J. Catal. 48 (1977) 87–97.
[2] H. Yasuda, Y. Fujiwara, N. Mizuno, M. Misono, J. Chem. Soc. Faraday Trans. 90 (1994) 1183–1189.
[3] B.P. Barbero, J.A. Gamboa, L.E. Cadús, Appl. Catal. B 65 (2006) 21–30.
[4] Y. Teraoka, H. Fukuda, S. Kagawa, Chem. Lett. 19 (1990) 1–4.
[5] Y. Teraoka, K. Nakano, W. Shangguan, S. Kagawa, Catal. Today 27 (1996) 107–113.
[6] H. Dai, H. He, P. Li, L. Gao, C.-T. Au, Catal. Today 90 (2004) 231–244.
[7] S. Royer, F. Bérubé, S. Kaliaguine, Appl. Catal. A 282 (2005) 273–284.
[8] R.J. Bell, G.J. Millar, J. Drennan, Solid State Ionics 131 (2000) 211–220.
[9] K. Rida, A. Benabbas, F. Bouremmad, M.A. Peña, A. Martínez-Arias, Catal. Commun. 7 (2006) 963–968.
[10] P.V. Gosavi, R.B. Biniwale, Mater. Chem. Phys. 119 (2010) 324–329.
[11] H.M. Zhang, Y. Teraoka, N. Yamazoe, Chem. Lett. 16 (1987) 665–668.

[12] K. Rida, A. Benabbas, F. Bouremmad, M.A. Peña, E. Sastre, M.A. -Arias, Appl. Catal. A 327 (2007) 173–179.
[13] W. Li, M.W. Zhou, J.L. Shi, Mater. Lett. 58 (2004) 365–368.
[14] M. Yuasa, K. Shimanoe, Y. Teraoka, N. Yamazoe, Catal. Today 126 (2007) 313–319.
[15] A.E. Giannakas, A.A. Leontiou, A.K. Ladavos, P.J. Pomonis, Appl. Catal. A 309 (2006) 254–262.
[16] Y. Teraoka, S. Nanri, I. Moriguchi, S. Kagawa, K. Shimanoe, N. Yamazoe, Chem. Lett. 29 (2000) 1202–1203.
[17] K. Tsuchida, S. Takase, Y. Shimizu, Sens. Mater. 16 (2004) 171–180.
[18] M. Popa, J. Frantti, M. Kakihana, Solid State Ionics 154–155 (2002) 437–445.
[19] I. Rossetti, L. Forni, Appl. Catal. B 33 (2001) 345–352.
[20] Y. Matuura, S. Matsushima, M. Sakamoto, Y. Sadaoka, J. Mater. Chem. 3 (1993) 767–769.
[21] Y. Sadaoka, E. Traversa, M. Sakamoto, Chem. Lett. 25 (1996) 177–178.
[22] Y. Sadaoka, E. Traversa, M. Sakamoto, J. Alloys Compd. 240 (1996) 51–59.
[23] M. Sakamoto, P. Nunziante, E. Traversa, S. Matsushima, M. Miwa, H. Aono, Y. Sadaoka, J. Ceram. Soc. Jpn. 105 (1997) 963–969.
[24] E. Traversa, P. Nunziante, M. Sakamoto, Y. Sadaoka, M.C. Carotta, G. Martinelli, J. Mater. Res. 13 (1998) 1335–1344.
[25] E. Traversa, P. Nunziante, M. Sakamoto, Y. Sadaoka, R. Montanari, Mater. Res. Bull. 33 (1998) 673–681.
[26] Y. Sadaoka, H. Aono, E. Traversa, M. Sakamoto, J. Alloys Compd. 278 (1998) 135–141.
[27] H. Aono, M. Sato, E. Traversa, M. Sakamoto, Y. Sadaoka, J. Am. Ceram. Soc. 84 (2001) 341–347.
[28] M. Asamoto, N. Harada, Y. Iwamoto, H. Yamaura, Y. Sadaoka, H. Yahiro, Top. Catal. 52 (2009) 823–827.
[29] Crystal Clear, Rigaku and Rigaku/MSC, The Woodlands, TX.
[30] Crystal Structure, Rigaku and Rigaku/MSC, The Woodlands, TX.
[31] M.C. Bulra, R. Cariandro, M. Camalli, B. Carrozzini, G.L. Cascarano, L. De Caro, C. Giatorazzo, G. Polidori, R. Spagna, SIR2004, 2005.
[32] G.M. Sherdric, SHELX97, Programs for Crystal Structure Analysis release 97-2, University of Göttingen, Göttingen, 1997.
[33] X. Zhou, W.T. Wong, M.D. Faucher, P.A. Tanner, J. Solid State Chem. 181 (2008) 3057–3064.
[34] Y. Itagaki, M. Mori, Y. Hosoya, H. Aono, Y. Sadaoka, Sens. Actuators B 122 (2007) 315–320.
[35] M. Asamoto, H. Yahiro, Catal. Surv. Asia 13 (2009) 221–228.
[36] S. Farhadi, Z. Momeni, M. Taherimehr, J. Alloys Compd. 471 (2009) 5–8.
[37] W. Xiaoyu, Y. Yukawa, Y. Masuda, J. Alloys Compd. 290 (1999) 85–90.
[38] M. Mori, Y. Iwamoto, M. Asamoto, Y. Itagaki, H. Yahiro, Y. Sadaoka, S. Takase, Y. Shimizu, M. Yuasa, K. Shimanoe, H. Kusaba, Y. Teraoka, Catal. Today 139 (2008) 125–129.